Dynamical Transition in the Open-boundary Totally Asymmetric Exclusion Process

A. Proeme, R. A. Blythe and M. R. Evans

SUPA, School of Physics and Astronomy, University of Edinburgh, Mayfield Road, Edinburgh EH9 3JZ, United Kingdom

E-mail: `arno.proeme@ed.ac.uk`, `r.a.blythe@ed.ac.uk`, `m.evans@ed.ac.uk`

Abstract. We revisit the totally asymmetric simple exclusion process with open boundaries (TASEP), focussing on the recent discovery by de Gier and Essler that the model has a dynamical transition along a nontrivial line in the phase diagram. This line coincides neither with any change in the steady-state properties of the TASEP, nor the corresponding line predicted by domain wall theory. We provide numerical evidence that the TASEP indeed has a dynamical transition along the de Gier–Essler line, finding that the most convincing evidence was obtained from Density Matrix Renormalisation Group (DMRG) calculations. By contrast, we find that the dynamical transition is rather hard to see in direct Monte Carlo simulations of the TASEP. We furthermore discuss in general terms scenarios that admit a distinction between static and dynamic phase behaviour.

Date: October 26, 2010

1. Introduction

As a rare example of a class of exactly-solvable, nonequilibrium interacting particle systems, asymmetric simple exclusion processes of various types have found favour with researchers in statistical mechanics, mathematical physics and probability theory [1–4]. These systems comprise hard-core particles hopping in a preferred direction on a one-dimensional lattice and have been used to describe systems as diverse as traffic flow [5], the dynamics of ribosomes [6] and molecular motors [7, 8], the flow of hydrocarbons through a zeolite pore [9], the growth of a fungal filament [10], and in queueing theory [11, 12]. The physical interest lies mainly in the rich phase behaviour that arises as a direct consequence of being driven away from equilibrium.

Of particular interest are the open boundary cases. Here the system can be thought of as being placed between two boundary reservoirs, generally of different densities. The two reservoirs enforce a steady current across the lattice, and therewith a nonequilibrium steady state. It was first argued by Krug [13] that as the boundary densities are varied nonequilibrium phase transitions may occur in which steady state bulk quantities— such as the mean current or density—exhibit nonanalyticities. Such phase transitions were seen explicitly in first a mean-field approximation [6, 14] and then in the exact solution [15, 16] of the totally asymmetric exclusion process with open boundaries, hereafter abbreviated as TASEP, and of related processes [4]. Since then arguments have been developed to predict the phase diagram of more general one-dimensional driven diffusive systems [17–19].

Our interest in this work is in the distinction between two phase diagrams for the TASEP: one of which characterises the steady-state behaviour, and the other the dynamics. The static phase diagram [15,16] is shown in Fig. 1(a) where the left boundary density is α and the right is $1 - \beta$. There are three possible phases in the steady state: a low density (LD) phase where the bulk density is controlled by the left boundary and is equal to α; a high density (HD) phase where the bulk density is controlled by the right boundary and is equal to $1 - \beta$; a maximal current (MC) phase where the bulk density is $\frac{1}{2}$. The high and low density phases are further divided into subphases (e.g. LD1, LDII) according to the functional form of the spatial decay of the density profile to the bulk value near the non-controlling boundary. In these subphases the lengthscale over which the decay is observable remains finite as the system size is increased. This change at the subphase boundaries in the form of the decay is thus not a true phase transition in the thermodynamic sense.

More recently, de Gier and Essler have performed an exact analysis of the ASEP's dynamics [20–22] and derived the the longest relaxation times of the system by calculating the gap in the spectrum using the Bethe ansatz. The analysis builds on directly related work on the XXZ spin chain with nondiagonal boundary fields [23, 24]. The dynamical phase diagram they obtain, in which phases are associated with different functional forms of the longest relaxation time, is illustrated in figure 1(b). The same phases (high density, low density and maximal current) are found as in the static phase
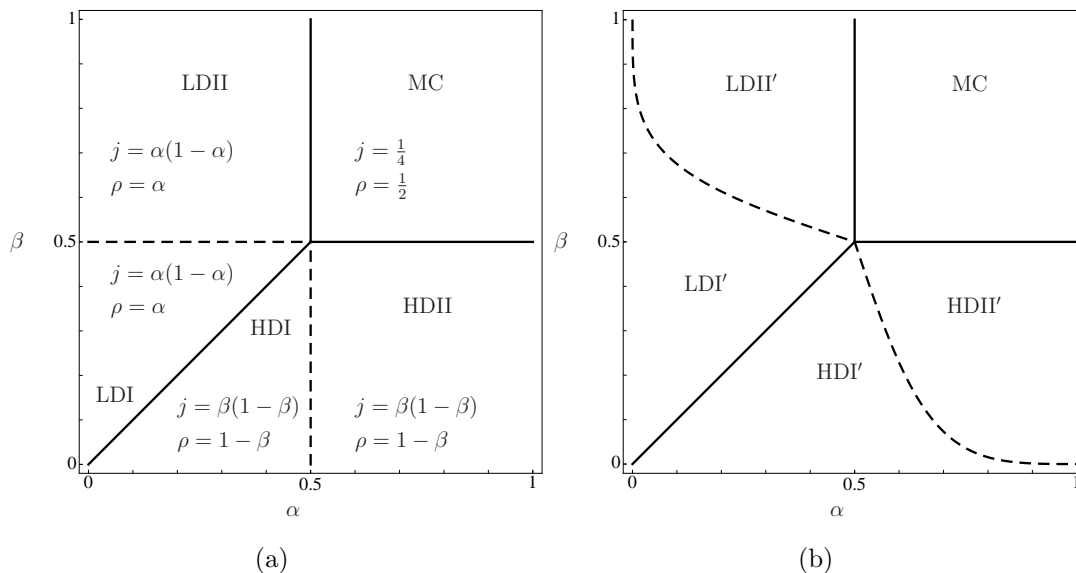
Figure 1. (a) Static and (b) dynamic phase diagrams for the TASEP. Solid lines indicate thermodynamic phase transitions at which the current and bulk density are nonanalytic. Dotted lines indicate subphase boundaries. In the static case, the density profile a finite distance from the boundary is nonanalytic. In the dynamic case, the longest relaxation time exhibits a nonanalyticity.

diagram, however, a hitherto unexpected *dynamical transition* line which subdivides the low density and high density phases is now apparent. This line which we shall refer to as the de Gier–Essler (dGE) line replaces the subphase boundaries at $\alpha = 1/2, \beta < 1/2$ $\beta = 1/2, \alpha < 1/2$ in the static phase diagram and, for example, subdivides the low density region into LDI′, LDII′.

Although there is nothing to rule out the prediction of dGE of a dynamical transition at a distinct location to any static transition, the result came as something of a surprise. This is because the static phase diagram had been successfully interpreted in terms of an effective, dynamical theory thought to be relevant for late-time dynamics, referred to as domain wall theory (DWT). We shall review DWT more fully in Section 2.4. For the moment we note that DWT correctly predicts the static subphase boundary and the associated change in the decay of the density profile, but does not predict the dGE line. Therefore, it was previously thought that a dynamical transition also occurred at the subphase boundary and initial calculations of relaxation times appeared to be consistent with this [25, 26].

Our primary goal in this work is to establish numerically that a dynamical transition does indeed occur along the dGE line rather than at the static subphase boundary. We used two distinct approaches. First, we carried out direct Monte Carlo simulations of the TASEP dynamics and identified the dominant transient in three time-dependent observables. We find that these simulations are consistent with a dynamical transition at the dGE line but are not sufficiently accurate to rule out the scenario of the dynamical transition occurring at the subphase boundary.

We instead turn to a Density Matrix Renormalisation Group (DMRG) approach [27] to acquire convincing evidence that a dynamical transition occurs at the dGE line. The DMRG is an approximate means to obtain the lowest-lying energies and eigenstates of model Hamiltonians with short-range interactions. Although originally developed in the context of the Hubbard and Heisenberg models [28] (see also [29] for a comprehensive review), it has also been applied to nonequilibrium processes such as reaction-diffusion models [30]. In particular, it has also been used to investigate the spectrum of the TASEP [26]. However, the dynamical transition was not evident from the data presented in that work—perhaps because it had not been predicted at that time. By revisiting this approach, we obtain estimates of the longest relaxation time that allow us to rule out the domain wall theory prediction for the dynamical transition.

The paper is organised as follows. We begin in Section 2 by recalling the definition of the TASEP, and by reviewing in more detail the static and dynamic phase diagrams discussed above. Then, in Section 3, we present our Monte Carlo simulation data, followed by the DMRG results in Section 4. In Section 5 we return to more general questions about the distinction between the static and dynamic phase diagram with particular reference to different theoretical approaches to the TASEP. We conclude in Section 6 with some open questions.

## 2. Model definition and phase diagrams

Although we have alluded to the basic properties of the totally asymmetric simple exclusion process (TASEP) in the introduction, in the interest of a self-contained presentation we provide in this section a precise model definition and full details of the static and dynamic phase diagrams.

2.1. Model definition

The TASEP describes the biased diffusion of particles on a one-dimensional lattice with L sites. No more than one particle can occupy a given site, and overtaking is prohibited. The stochastic dynamics are expressed in terms of transition rates, for example a particle on a site i in the bulk hops to the right as a Poisson process with rate 1, but only if site $i + 1$ is unoccupied: At the left boundary only particle influx takes place, with rate α, and at the right boundary only particle outflux takes place, with rate β, as shown in Fig. 2. The corresponding reservoir densities are α at the left and $1 - \beta$ at the right.

2.2. Static phase diagram

As noted in the introduction, the TASEP static phase diagram can be determined from, for example, exact expressions for the current and density profile in the steady state [15,16]. The current takes three functional forms according to whether it is limited by a slow insertion rate (LD: $\alpha < \beta, \alpha < \frac{1}{2}$), by a slow exit rate (HD: $\beta < \alpha, \beta < \frac{1}{2}$) or by the exclusion interaction in the bulk (MC: $\alpha > \frac{1}{2}, \beta > \frac{1}{2}$). This behaviour of
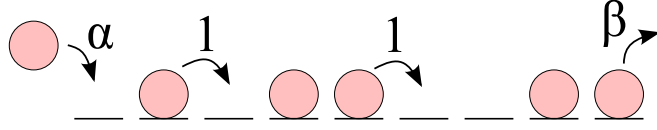
Figure 2. The dynamics of the totally asymmetric simple exclusion process (TASEP) with open boundaries. Arrows show moves that may take place, and the labels indicate the corresponding stochastic rates.

the current leads to the identification of the thermodynamic phases separated by solid lines in Fig. 1(a). Along these lines there are nonanalyticities in both the current and the density far from either boundary. The relevant expressions for these quantities are shown on Fig. 1(a).

The density *near* one of the boundaries is nonanalytic along the lines $\alpha = \frac{1}{2}$ and $\beta = \frac{1}{2}$ in the HD and LD phases respectively. These subphases are shown dotted in Fig. 1(a). Inspection of the functional form of the density profile reveals that these are not true thermodynamic phase transitions, in the sense that the deviation from the bulk value extends only a finite distance into the bulk, and thus contributes only subextensively to the nonequilibrium analogue of a free energy (see e.g., [31] for the definition of such a quantity). To be more explicit, consider for example the behaviour near the right boundary in the low-density phase. Here the bulk density is $\rho = \alpha$. The mean occupancy of the lattice site positioned a distance j from the right boundary approaches in the thermodynamic limit $L \to \infty$ the form [4, 15, 16]

$$\rho_{L-j} \sim \begin{cases} \alpha + c_{\mathrm{I}}(\beta) \left(\frac{\alpha(1-\alpha)}{\beta(1-\beta)} \right)^{j} & \alpha < \beta < \frac{1}{2} \qquad (\mathrm{LDI}) \\ \alpha + c_{\mathrm{II}}(\alpha, \beta) \frac{[4\alpha(1-\alpha)]^{j}}{j^{3/2}} & \frac{1}{2} < \beta \qquad (\mathrm{LDII}) \end{cases} \tag{1}$$

In these expressions, c_{I} and c_{II} are functions of the boundary parameters that we leave unspecified here so as to focus on the lengthscale of the exponential decay from the right boundary. As β is increased from zero, the decay length increases until $\beta = \frac{1}{2}$. Then the decay length is constant, and the exponential is modulated by a power law. The density profile at the left boundary exhibits the same kind of nonanalyticity in the high-density phase as α is increased through $\frac{1}{2}$ as a consequence of the particle-hole symmetry, $\rho_{i-1}(\alpha, \beta) = 1 - \rho_{L-i}(\beta, \alpha)$, exhibited by the model.

2.3. Dynamical phase diagram

The dynamic phase diagram is obtained by examining a quantity referred to as the *gap* by de Gier and Essler [20–22]. This is simply the largest nonzero eigenvalue of the transition matrix governing the continuous-time stochastic dynamics of the TASEP. More formally, one starts with the master equation

$$\frac{\mathrm{d}}{\mathrm{d}t} |P(t)\rangle = M |P(t)\rangle \,, \tag{2}$$

where the matrix M encodes the transition rates and $|P(t)\rangle$ is the vector of probabilities for each configuration. Because M is a stochastic matrix it is guaranteed [32] by the

Perron-Frobenius theorem to have eigenvalues satisfying

$$\lambda_0 = 0 > \mathrm{Re}(\lambda_1) \geq \mathrm{Re}(\lambda_2) \geq \dots . \tag{3}$$

The spectrum corresponds to a set of relaxation times $\tau_i = -(\mathrm{Re}\,\lambda_i)^{-1}$. The longest (non-infinite) relaxation time is τ_1, and the associated eigenvalue λ_1 is the gap which we will henceforth denote by the symbol ε. At long times the relaxation of any observable is expected to decay exponentially with a characteristic timescale τ_1, a fact we will later use to estimate the gap from Monte Carlo simulations.

The thermodynamic phase boundaries are found by identifying lines along which the gap vanishes, indicating the coexistence of two stationary eigenstates (phases). The exact calculations of de Gier and Essler [20, 21] show that, in the thermodynamic limit $L \to \infty$, the gap vanishes along the line $\alpha = \beta < \frac{1}{2}$ that separates the HD and LD phases. The gap also vanishes in the entirety of the MC phase, reflecting the generic long-range (power-law) correlations seen in this phase [15]. Thus at this level, the static and dynamic phase diagrams coincide.

Where they differ is in the subdivision of the high- and low-density phases‡, in which the gap remains finite in the limit $L \to \infty$. There is a region, marked LDI′ and HDI′ on Fig. 1(b), within which the gap assumes the asymptotic expression

$$\varepsilon(L) = -\alpha - \beta + \frac{2}{(ab)^{\frac{1}{2}} + 1} - \frac{\pi^2}{(ab)^{\frac{1}{2}} - (ab)^{-\frac{1}{2}}} L^{-2} + \mathcal{O}(L^{-3}) \tag{4}$$

in which

$$a = \frac{1-\alpha}{\alpha} \quad \text{and} \quad b = \frac{1-\beta}{\beta} . \tag{5}$$

Within the low-density phase ($\alpha < \beta, \alpha < \frac{1}{2}$), this form of the gap applies for values of $\beta < \beta_c$ where

$$\beta_c(\alpha) = \left[1 + \left(\frac{\alpha}{1-\alpha} \right)^{\frac{1}{3}} \right]^{-1} . \tag{6}$$

Likewise, in the high-density phase ($\beta < \alpha, \beta < \frac{1}{2}$), the region within which the gap is given by (4) is bounded by $\alpha < \alpha_c$ where

$$\alpha_c(\beta) = \left[1 + \left(\frac{\beta}{1-\beta} \right)^{\frac{1}{3}} \right]^{-1} . \tag{7}$$

In the remainder of the low-density phase, $\alpha < \frac{1}{2}, \beta > \beta_c$ the gap takes the form

$$\varepsilon(L) = -\alpha - \beta_c + \frac{2}{(ab_c)^{\frac{1}{2}} + 1} - \frac{4\pi^2}{(ab_c)^{\frac{1}{2}} - (ab_c)^{-\frac{1}{2}}} L^{-2} + \mathcal{O}(L^{-3}) . \tag{8}$$

Finally, we have by symmetry that when $\beta < \frac{1}{2}, \alpha > \alpha_c$,

$$\varepsilon(L) = -\alpha_c - \beta + \frac{2}{(a_c b)^{\frac{1}{2}} + 1} - \frac{4\pi^2}{(a_c b)^{\frac{1}{2}} - (a_c b)^{-\frac{1}{2}}} L^{-2} + \mathcal{O}(L^{-3}) . \tag{9}$$

‡ de Gier and Essler [20–22] refer to these as "massive" phases by analogy with the quantum spin chains; we shall only use the terminology associated with the static phase diagram to avoid confusion.
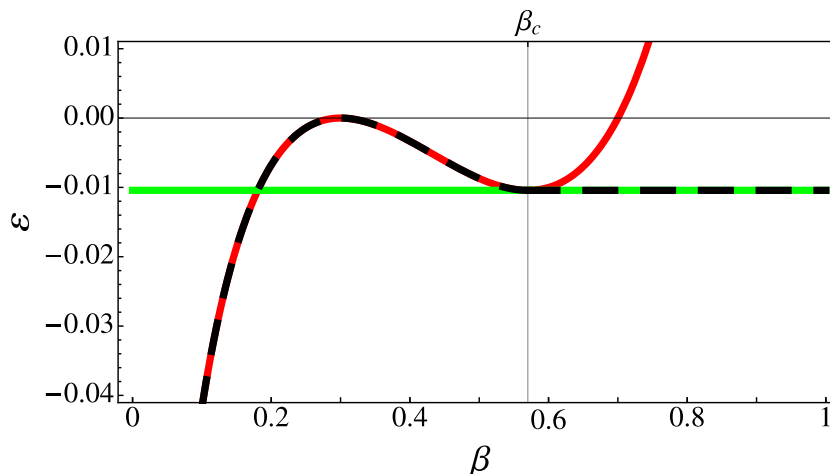
Figure 3. Exact $L \to \infty$ gap (black, dashed) as a function of β for $\alpha = 0.3$, described by the HDI$'$ equation (4) (red) for $\beta < \beta_c$ ($\beta_c \approx 0.57$, indicated), and by equation (8) (green) for $\beta > \beta_c$.

In these expressions,

$$a_c = \frac{1 - \alpha_c}{\alpha_c} \quad \text{and} \quad b_c = \frac{1 - \beta_c}{\beta_c} \; . \tag{10}$$

The boundaries between the dynamic subphases—the de Gier–Essler (dGE) lines—are shown dotted in Fig. 1(b). Note that the coefficient of the L^{-2} term in this asymptotic expansion is discontinuous across the dynamical transition line.

In order to illustrate the behaviour of the gap along the static and dynamic transition lines, we plot it as a function of β at some $\alpha < \frac{1}{2}$ in Fig. 3. The most striking feature is the constancy of the gap above the nontrivial critical point β_c. Later in this work, we will use the constancy of the gap above a critical threshold as an empirical means to identify the dynamical transition point.

2.4. Domain wall theory

An alternative approach to study the TASEP dynamics is domain wall theory (DWT) [33]. Although much simpler than the Bethe ansatz approach of de Gier and Essler, it correctly predicts the static phase boundaries and the analytical form of the gap in a region of the phase diagram. However, it predicts dynamic subphases that are distinct from those found by de Gier and Essler, and that correspond to the static subphases. In the numerical study that follows, it will be important to be able to distinguish between these two sets of predictions, and so we summarise DWT here.

The basis of this approach is to assume that collective relaxational dynamics are effectively reducible to a single coordinate describing the position of an interface, or domain wall. The wall separates a domain of density ρ^- and current j^- to the left from a domain of density ρ^+ and current $j^+ = \rho^+(1 - \rho^+)$ to the right. Each domain is taken to possess the steady state characteristics imposed by the boundary reservoir on that
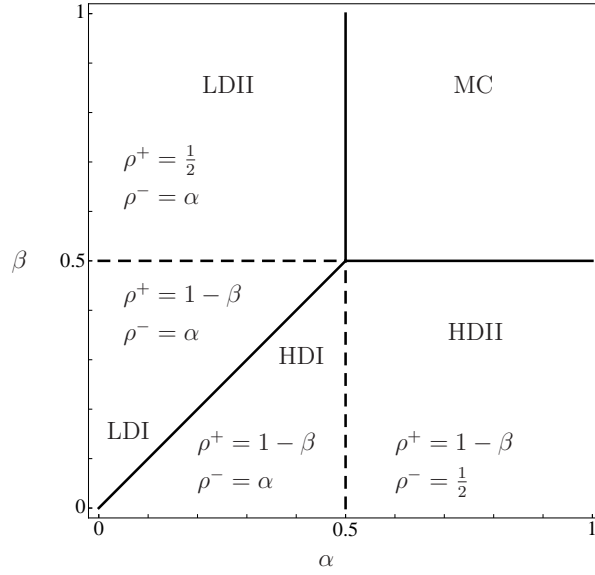
Figure 4. The phase diagram obtained from domain wall theory. ρ^+ and ρ^- indicate the densities of the left and right domains. In the domain wall theory, static and dynamic transitions coincide along the dashed lines.

particular side of the wall, with ρ^+ and ρ^- therefore as in Fig. 4. The effective theory is expected to be exact along the line $\alpha = \beta < 1/2$ where the exact properties of the system such as density profile [15, 16] and current fluctuations [34] are recovered.

Let us consider the case $\alpha < 1/2$ and $\beta < 1/2$. The motion of the wall is then described microscopically as a random walker with left and right hopping rates D^- and D^+ given respectively by imposing mass conservation on the fluxes into and out of the wall [25]:

$$D^- = \frac{j^-}{\rho^+ - \rho^-} = \frac{\alpha(1-\alpha)}{1-\alpha-\beta} \qquad D^+ = \frac{j^+}{\rho^+ - \rho^-} = \frac{\beta(1-\beta)}{1-\alpha-\beta}, \tag{11}$$

For $\alpha > \beta$ the random walk is biased to the left and in the stationary state the domain wall is localised at the left boundary and the bulk density is given by $\rho^+ = 1 - \beta$. For $\alpha < \beta$ the random walk is biased to the right and in the stationary state the domain wall is localised at the right boundary and the bulk density is given by $\rho^- = \alpha$. Thus the first order transition at $\alpha = \beta$ is correctly predicted.

Moreover, the gap in the resulting spectrum for large L given [25] is given by

$$\varepsilon_{DWT} = -D^+ - D^- + 2\sqrt{D^+ D^-}\left(1 - \frac{\pi^2}{2L^2} + O(L^{-3})\right). \tag{12}$$

Remarkably this expression is identical to (4) to order $1/L^2$. Thus in the region $\alpha < 1/2, \beta < 1/2$ DWT correctly predicts the gap.

When $\beta > 1/2$ so that $\rho^+ = 1/2$, one can take j^+ in (11) to depend on the size ℓ of the right-hand domain. That is, one puts $j^+ \to j^+(\ell)$ equal to the stationary current in a TASEP of size ℓ in the maximal current phase. This implies the large ℓ behaviour

$$j^+ \simeq \frac{1}{4}\left(1 + \frac{3}{2\ell}\right) \tag{13}$$
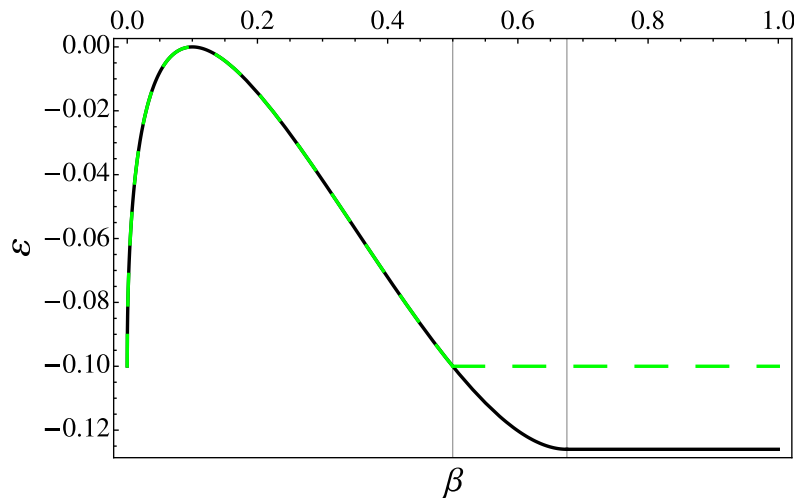
Figure 5. Comparison of the gap for $L \to \infty$ from domain wall theory (dashed line) with the exact gap (solid line) at $\alpha = 0.1$ (for which $\beta_c \approx 0.675$).

This results in a modification of the density profile to an exponential spatial decay modulated by a power law with power $3/2$, similar to Eq. 1 (LDII).

In brief, the DWT is remarkably successful, correctly predicting the static phase diagram (including subphases), and the exact thermodynamic gap function found by de Gier and Essler in the region $\alpha < 1/2$ and $\beta < 1/2$. It differs in that the dynamic subphases are not given by the dGE lines, but the static subphase transition lines. Thus, the region within which the gap is constant is different in the two theories, as indicated by Fig. 5.

3. Evidence for the dynamical transition from Monte Carlo simulations

We now describe attempts to measure the gap in Monte Carlo simulations of the TASEP, with a particular interest in distinguishing between the dGE and DWT predictions. As noted previously, the ensemble average of any time-dependent observable $\mathcal{O}(t)$ should be dominated at late times by an exponential decay $\mathrm{e}^{-|\lambda_1|t}$ to its stationary value $\langle \mathcal{O} \rangle$. Recall that λ_1 is the largest nonzero eigenvalue of the matrix M appearing in the master equation (2), and that all nonstationary eigenvalues have negative real part. In principle, therefore, all one needs to do is pick an observable, and measure its late-time decay rate. In practice, this is made difficult by the fact that *all* decay modes may contribute to $\langle \mathcal{O}(t) \rangle$, and that by the time the higher modes have decayed away, the residual signal $\langle \mathcal{O}(t) \rangle - \langle \mathcal{O} \rangle$ may be extremely small and swamped by the noise.

Since we are interested in the time-dependence of an observable, we employ a *continuous-time* (Gillespie) algorithm [35] to simulate the TASEP dynamics. More precisely, we maintain a list of events (i.e., a particle hopping to the next site, or entering or leaving the system) that can take place given the current lattice configuration. A particular event i is then chosen with a probability proportional to its rate ω_i as specified in Section 2. A time variable is then incremented by an amount chosen from

an exponential distribution with mean $(\sum_i \omega_i)^{-1}$. In this way, a member of the ensemble of all continuous-time trajectories of the TASEP dynamics from some prescribed initial condition is generated with the appropriate probability.

3.1. Decay of total occupancy to stationarity

We consider first the decay of the total number of particles on the lattice, $N(t)$, to its stationary value as measured by the function

$$R(t) = \frac{\langle N(t) \rangle - \langle N \rangle}{\langle N(0) \rangle - \langle N \rangle} . \tag{14}$$

In this expression, angle brackets denote an average over an ensemble of initial conditions and over stochastic trajectories. In each simulation run, an initial condition was constructed in which each site was independently occupied with a probability $p = 1 - \beta$ (in the LD phase) or $p = \alpha$ (in the HD phase). In the bulk, these densities then relax to the steady-state values displayed on Fig. 1(a).

Once $R(t)$ has been sampled over multiple trajectories, the task is to identify a time window over which one can fit an exponential decay and therewith estimate a gap. The start and end points of this windows are both crucial. If it starts too early, then one may expect contributions from subdominant transients (i.e., the decays at rate $\lambda_2, \lambda_3, \ldots$) to systematically skew the estimate of the gap. If it ends too late, noise may instead dominate the estimate.

The noise at the top end we handle by examining the behaviour of local decay rates

$$\mu_i = \frac{\ln R(t_{i+i}) - \ln R(t_i)}{t_{i+1} - t_i} \tag{15}$$

where t_i and t_{i+1} are successive time points at which $R(t)$ was sampled. At late times, one should find $\mu_{i+1}/\mu_i \to 1$. Strong deviations from unity indicate the dominance of noise, and we rejected points after which the magnitude of this ratio exceeded a critical value. For our data sets, we found that 5 was a suitable choice for this value: see Fig. 6(a) for an example.

The bottom end of the window was chosen by maximising a goodness-of-fit measure to a fit of the exponential $f(t) = a e^{-\lambda t}$ to data points within the window. We adopted the *adjusted coefficient of determination* [36]

$$\mathcal{R}^2 = 1 - \frac{\frac{1}{n-k} \sum_i (R(t_i) - f(t_i))^2}{\frac{1}{n-1} \sum_i (R(t_i) - \bar{R})^2} . \tag{16}$$

as our goodness-of-fit measure, varying the start of the window until this quantity was maximised. In this expression $\bar{R}$ is the arithmetic mean of $R(t)$ over the set of n times t_i falling within the window, and k is the number of free parameters in the fit function $f(t)$, i.e., $k = 2$. This goodness-of-fit measure trades off the increased quality of the fit obtained by discarding data points against the increasing uncertainty in the fitting parameters that comes with the noisier data at the top end of the window. We show in Fig. 6(b) an example of how the goodness-of-fit varies with the size of the window.

(a)

(b)
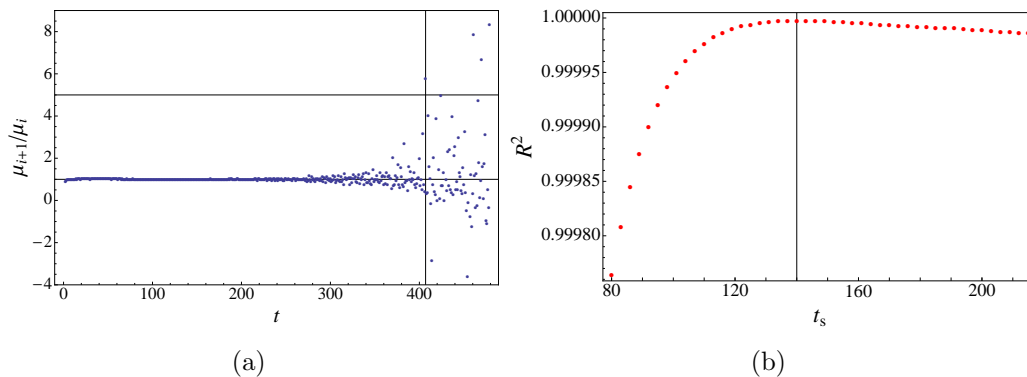
Figure 6. Criteria for choosing the range of data over which to fit a single exponential to the decay of the density to stationarity. (a) The ratio of gradients μ_{i+1}/μ_i which should be close to unity where a single exponential is a good fit. At large times, this ratio becomes noisy; the presence of extreme values (here, a magnitude larger than 5) is used to identify the onset of noise. (b) The behaviour of $\mathcal{R}^2$ as a function of the start of the window. We choose this such that $\mathcal{R}^2$ is maximised. In both cases, $L = 50$, $\alpha = 0.3$ and $\beta = 0.64$.

We remark that the relative flatness of $\mathcal{R}^2$ above the optimal starting time can be ascribed to the fact that only a single decay mode remains in this region. Although this procedure is a little cumbersome to apply to each data set, we found it preferable to fitting multiple exponentials to the data for $R(t)$, which leads to large uncertainties in the measured gap.

We show results in Fig. 7, in which the gap is plotted as a function of β for fixed $\alpha = 0.3$ for a range of system sizes. At the smallest system sizes ($L = 10$) data from Monte Carlo simulation are in agreement with results obtained through exact diagonalisation of the matrix M. As the system size is increased beyond the sizes for which exact techniques remain tractable, the curves approach those predicted by dGE and DWT. However, it is not possible to discern from the largest system simulated, $L = 150$, which of these theories is more appropriate.

We therefore attempt to extrapolate to the limit $L \to \infty$ by fitting a function of the form $\varepsilon + a_2 L^{-2} + a_3 L^{-3} + a_4 L^{-4}$ to estimates of the gap at finite system sizes L but fixed α and β. This particular fitting function was found to have the best goodness-of-fit (taking into account the varying number of parameters) out of those that were tried, and furthermore had the most uniform goodness-of-fit as a function of β. The results of this extrapolation procedure are shown in Fig. 8. These data appear to exclude the functional form for the domain wall theory, although the uncertainties in the estimated gaps are such that further evidence is needed in order to confidently rule it out.

3.2. Decay of other observables

One possible means to reduce the uncertainty in the measured gap is to try different observables $\mathcal{O}(t)$ in the hope that contributions from subdominant decay modes—and in particular the second longest-lived mode that decays at rate λ_2—are reduced and
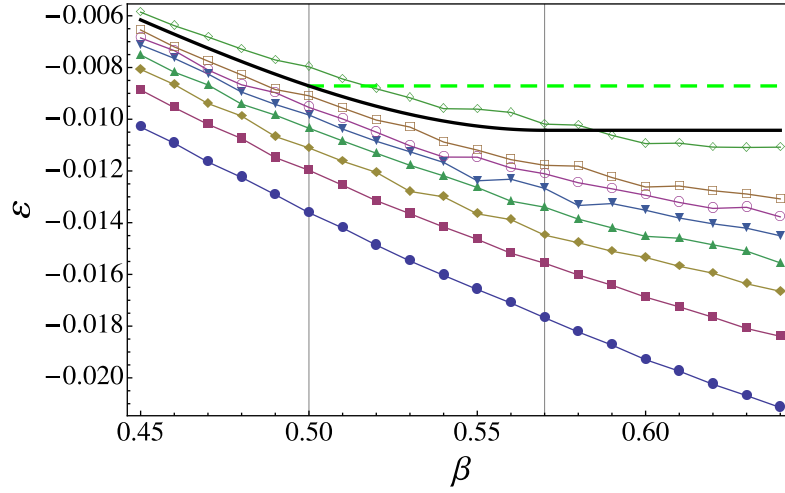
Figure 7. The gap as a function of β at $\alpha = 0.3$ and system sizes L ranging from $L = 40$ to $L = 150$ (from bottom to top) obtained from Monte Carlo simulations. The $L \to \infty$ dGE (solid line) and DWT (dashed line) predictions are shown for comparison: even with the largest system $L = 150$ simulated, one cannot distinguish between them numerically.
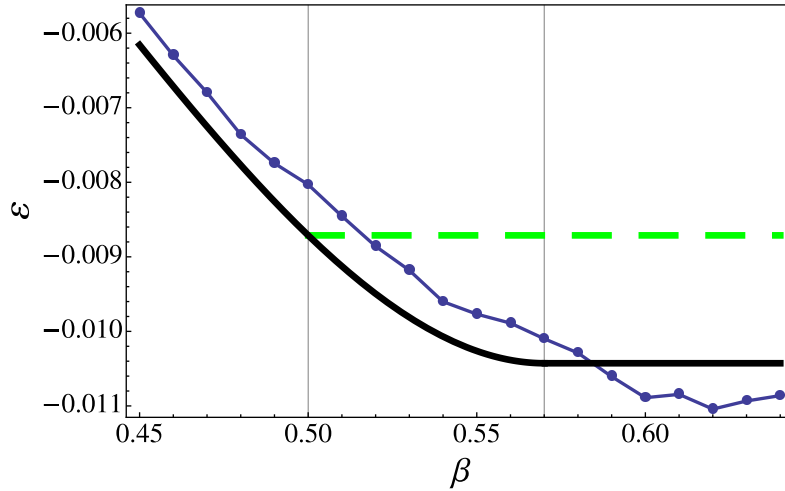

Figure 8. The gap extrapolated to $L = \infty$ from the data shown in Fig. 7. Again the dGE (solid line) and DWT (dashed line) predictions are shown for comparison: here the data are potentially more compatible with the former than the latter.

thereby allow a more accurate estimate of λ_1. We considered two candidates.

The first was the autocorrelation function of the total occupancy, $\mathcal{O}(t) = N(t_0)N(t_0 + t)$, where t_0 is some fixed time point in the steady state. The analogue of the function $R(t)$ is

$$\chi(t) = \frac{\langle N(t_0 + t)N(t_0)\rangle - \langle N\rangle^2}{\langle N^2\rangle - \langle N\rangle^2} \tag{17}$$

where here all averages are taken in the steady state. Numerically, this quantity is
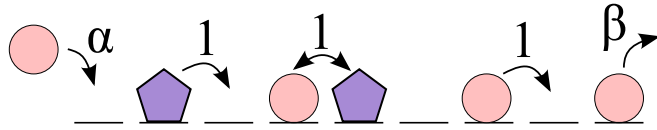
Figure 9. Interactions between first class (circles) and second class (hexagons) particles. Second class particles hop can forward into empty sites and exchange places with first-class particles behind them. Note that in our simulations, at most one second-class particle was present at any instant, and that the behaviour at the boundaries was chosen so as not to affect the motion of first-class particles (see text).

slightly more convenient than $N(t)$, since one can obtain $\langle N(t_0 + t)N(t_0)\rangle$ by sampling at different t_0 and t from a single simulation run that has reached the steady state.

The other observable we investigated was the position of a second class particle [37–39]. Like a first-class particle, a second-class particle hops to the right into vacant sites. However, it may also exchange places with a particle occupying the site to its left. Both of these processes take place at unit rate, and first-class hop to the right at the same rate, irrespective of whether the site in front of them is empty or occupied by a second-class particle—see Fig. 9. So as not to affect the entry of first-class particles into the system, a second-class particle on the left-boundary site is forced to exit if a first-class particle attempts to enter. It is reinserted as soon as the left-boundary site becomes vacant again. Second-class particles are prevented from exiting at the right boundary. In these simulations one can measure the position of the second class particle, $x(t)$, starting from an initial condition where each site is occupied by a first-class particle with density ρ (as described above) except for the left boundary site, which is always initially occupied by the second-class particle. Here, the analogue of $R(t)$ is

$$\xi(t) = \frac{\langle x(t)\rangle - \langle x\rangle}{x(0) - \langle x\rangle} \ . \tag{18}$$

Gaps obtained from these two functions $\chi(t)$ and $\xi(t)$ are compared with those obtained from $R(t)$ in Fig. 10 at various system sizes. We see that there are no systematic differences between these functions at the system sizes studied, and therefore that they are unlikely to provide improved estimates of the gap in the thermodynamic limit $L \to \infty$. We therefore conclude that whilst Monte Carlo simulation data is possibly more consistent with the de Gier–Essler prediction for the gap than the domain wall theory, the effect of the changing gap on the relaxation of a typical observable is very small and hard to disentangle from the noise.

4. Evidence for the dynamical transition from density matrix renormalisation

Given the difficulties in measuring the gap from Monte Carlo simulations, we now turn to a fundamentally different numerical approach, namely the density matrix renormalisation group (DMRG) [27] that was briefly discussed in the introduction.
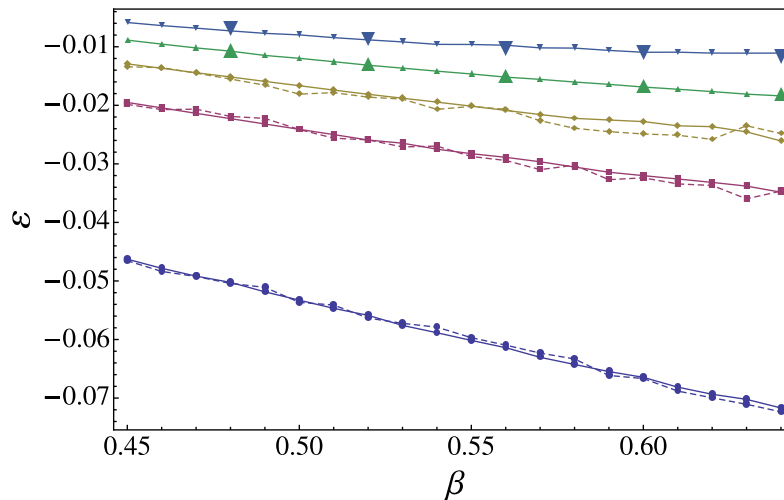
Figure 10. The gap as a function of β as obtained by consideration of the relaxation of three different observables. Solid lines show data obtained from the relaxation of the density for system sizes $L = 10, 20, 30, 50, 150$ (bottom to top). Alongside the lower three curves are plotted data from the stationary density auto-correlation function (17) (dashed lines), and alongside the upper two data from the position of a single second-class particle (18) (large symbols). All three observables yield consistent results.

We begin by recapitulating the essential features of the DMRG approach before demonstrating that it does indeed show a dynamical transition along the de Gier–Essler line.

4.1. DMRG algorithm for the TASEP gap

The density matrix renormalisation group (DMRG) procedure builds an approximation to the transition matrix M that appears in the master equation (2). The basic idea is to repeatedly add sites to the system and renormalise the enlarged transition matrix so that its dimensionality remains constant as the system size grows. In this way, the approximated transition matrix remains sufficiently small that its spectrum (and in particular the gap) can be determined using standard numerical diagonalisation methods. The success of this procedure relies on finding a reduced basis set at each renormalisation step that allows the lowest-lying eigenstates to remain well approximated as sites are added.

Since the TASEP has open boundaries, the extension of the lattice is achieved in this instance by adding sites to the *middle* of the system rather than at one of the ends [26]. The system is thus divided into two 'blocks': the left and right halves of the lattice. It is extended in each iteration by adding a site at the right-hand end of the left block, and the left-hand end of the right block. In order to understand the results that come out of the procedure, it is worth explaining in a little more detail how the renormalisation is actually achieved—full details are provided in Appendix A.

We outline the procedure in terms of the transformation applied to the left block.
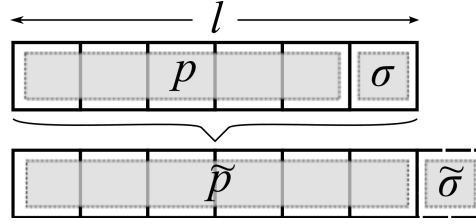
Figure 11. Illustration of the DMRG procedure applied to the left block. Before the transformation, the state of the block is specified by $1 \leq p \leq m$ and $\sigma = 0, 1$. After adding a new site to the end of the block, the original ℓ sites are renormalised so that they are specified by the two numbers $1 \leq \tilde{p} \leq m$ and $\tilde{\sigma} = 0, 1$. The right block is a mirror image of the left, and treated the same way.

Suppose that at the start of the iteration, the block comprises ℓ lattice sites. The set of states the block can be in is specified by two 'quantum' numbers, $p = 1, 2 \ldots, m$ and $\sigma = 0, 1$. The quantity p indexes the configuration of the first $\ell - 1$ sites, and σ the occupancy of the rightmost site. The first step of the renormalisation is to construct some basis in the $2m$-dimensional space spanned by p and σ and, crucially, retain only m of these basis vectors. This defines a renormalised index $\tilde{p} = 1, 2, \ldots, m$ for the *entire* ℓ-site block. A new site is then added to the right hand side of the lattice. The configuration of this additional site is specified by the renormalised coordinate $\tilde{\sigma}$. See Fig. 11. The reason for keeping the rightmost site in the 'physical' (site occupancy) basis is that one needs to project the transition matrix for hops from site ℓ to $\ell + 1$ onto the space spanned by $\tilde{p}$ and $\tilde{\sigma}$. These transition rates are initially only known in this physical basis. Thus through this procedure, we obtain a (truncated) representation of the transition matrix for an $\ell + 1$-site system in a space of the same dimensionality as that used to describe the ℓ-site system.

The same transformation is applied to the right block, the only difference being that it is the leftmost site that is expressed in the physical basis. Interactions between the two blocks enter through the construction of the renormalised indices $\tilde{p}$ as we now describe. First, a transition matrix M' for the entire system of 2ℓ sites is constructed by combining the matrices for the two halves, and by adding an interaction term that allows a particle in the left block to hop to the right block. Again, having the internal two sites specified in the physical basis helps here. This transition matrix is then diagonalised. However, it is not these eigenstates that are used to perform the renormalisation. Rather, a *density matrix*, which is a symmetric combination of the two longest-lived eigenstates of M', is constructed, and eigenvectors of this density matrix are instead used for the renormalisation. The idea is that this form of the density matrix allows the stationary and longest-lived transient state to be accurately represented in large systems. The specific form of the density matrix, and the prescription for obtaining the truncated basis set, is given in Appendix A. For further details about the principles behind DMRG and other applications we refer to [27, 40, 41], and especially [29].
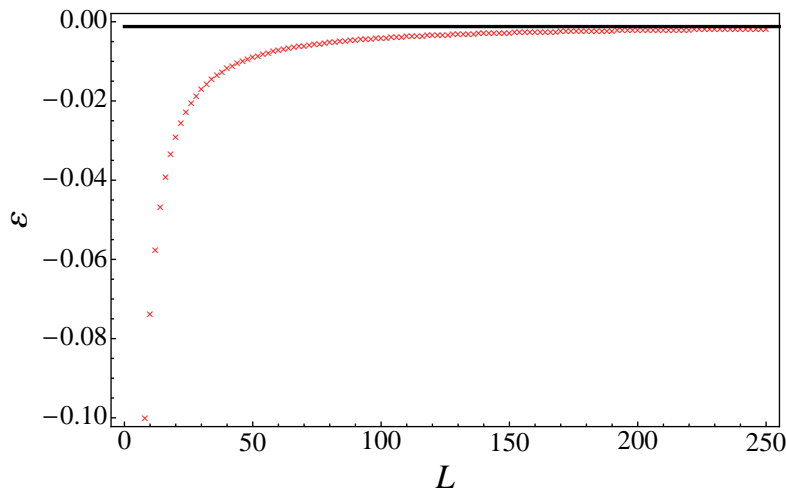
Figure 12. Stable DMRG data for the gap (red crosses) and the exact thermodynamic gap (black line) at $\alpha = 0.4$ and $\beta = 0.75$.

4.2. DMRG results

We used the DMRG algorithm outlined above to estimate the gap for a given combination of α and β by starting with an exact diagonalisation of the $L = 8$ system, and keeping $m = 16$ eigenvectors of the density matrix in each renormalisation step. In principle, one ought to be able to access arbitrarily large system sizes with this method. In practice—and as was also noted in [26]—the algorithm eventually goes unstable, which is typically manifested through the gap acquiring an imaginary part. We simply ignore data for system sizes where the instability is judged to have kicked in.

Although we can access larger system sizes with the DMRG approach than was possible with Monte Carlo (e.g., L up to about 250, as shown in Fig. 12), it is still necessary to extrapolate to the thermodynamic limit, $L \to \infty$. We follow a similar procedure to that described in Section 3.1. That is, we specify a finite-size fitting function of the form $f(L) = \varepsilon + a_2 L^{-2}$, and adjust the smallest value of L used for the fit. Again, we use $\mathcal{R}^2$ as a goodness-of-fit measure, i.e., Eq. (16) with t replaced by L. We show in Fig. 13(a) how the goodness of fit varies with the minimum value of L used in the fit; choosing the optimal (largest) value yields an estimate of the gap that we observe from Fig. 13(b) that appears more consistent with the de Gier–Essler prediction than domain wall theory.

We show the DMRG estimate of the gap obtained in this way as a function of β in Fig. 14. The agreement with the analytical prediction common to dGE and DWT below $\beta < \frac{1}{2}$ is very good. For larger β the data are scattered around an apparently constant value, indicating the presence of inaccuracies in the DMRG algorithm and/or the extrapolation of $L \to \infty$. If we regard these data as independent measurements of the same value, we can obtain an estimate of the uncertainty in the constant value of the gap above some critical point by simply calculating the standard deviation. We find the DMRG gap to approach the constant value $\varepsilon = -0.00125(9)$ when $\alpha = 0.4$. For
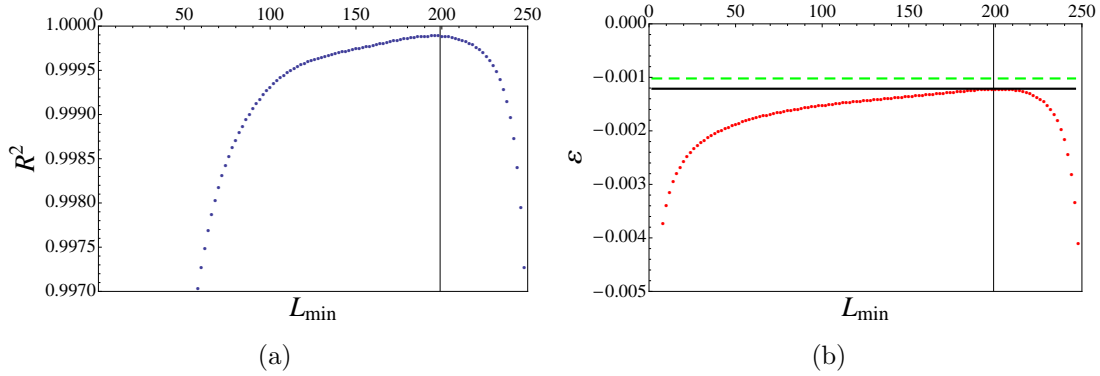
Figure 13. (a) Coefficient of determination R^2 and (b) extrapolated gap, as a function of $L_{\min}$ for DMRG data corresponding to $\alpha = 0.4$, $\beta = 0.75$. The optimal choice of $L_{\min}$ lies just below 200, for which the extrapolated gap very closely matches the de Gier-Essler result and clearly differs from the DWT gap.
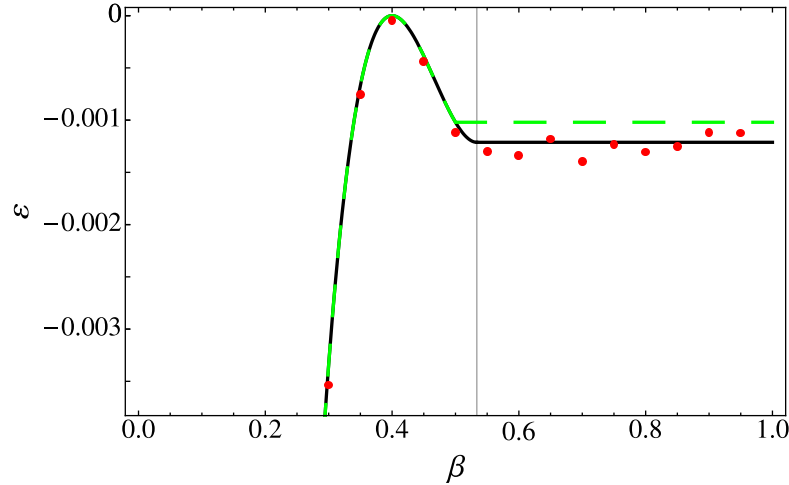
Figure 14. DMRG estimates of the gap (red crosses), exact thermodynamic gap (black curve) and DWT gap (green curve), all as a function of β at $\alpha = 0.4$ (for which $\beta_c \approx 0.53$).

comparison, de Gier and Essler predict a constant value for the gap of $-0.00121\ldots$ above the dynamical transition, while domain wall theory predicts $-0.00102\ldots$. The DMRG measurement is then clearly consistent with the de Gier–Essler prediction, whilst the difference from the domain wall theory value is significant. Taking this result together with the Monte Carlo data we conclude that a dynamical transition does indeed occur at the dGE line, and not where DWT predicts.

5. Discussion of the distinction between static and dynamic subphases

In this paper we have presented numerical evidence, the most convincing of which came from DMRG calculations, that a dynamical transition occurs in the TASEP at the dGE line rather than at the subphase boundary. However, this finding in turn raises

a number of open questions. For example, does the dGE line—and in particular its departure from the static subphase boundary—have any physical significance? How is the static subphase boundary manifested in the eigenvalue spectrum? We discuss the distinction between the two phase diagrams first in general theoretical terms, and then with reference to different treatments of the TASEP.

5.1. General theory of nonequilibrium phase transitions

One way to gain a general understanding of nonequilibrium phase transitions is through the analogue of partition function for a system of size L, Z_L [31, 32]. It has been shown that for any system governed by Markovian dynamics, it may be written as

$$Z_L = \prod_{j \neq 0} (-\lambda_j) \tag{19}$$

where $(-\lambda_j)$ are the eigenvalues of the Markov transition matrix which defines the dynamics [32, 42]. For a finite, irreducible configuration space there is a unique stationary state corresponding to the largest eigenvalue $\lambda_0 = 0$. By the Perron-Frobenious theorem [43], λ_0 is non-degenerate, therefore the gap is given by the second largest eigenvalue λ_1 and the largest relaxation time is $\tau_1 = -1/\lambda_1$.

From our knowledge of equilibrium phase transitions, we expect a static phase transition to occur when $\lim_{L \to \infty} \frac{1}{L} \ln Z_L$ exhibits nonanalyticities. We see from (19) that to obtain a static phase transition we require a major restructuring of the eigenvalue spectrum. To be general and explicit let us consider the nonequilibrium analogue of the free energy density,

$$h_L = \frac{\ln Z_L}{L} = \frac{1}{L} \sum_{\lambda_i \neq 0} \ln(-\lambda_i) . \tag{20}$$

Consider an arbitrary eigenvalue λ_i in (20), possessing a nonanalyticity at a critical value of some parameter. Unless a significant number of other eigenvalues in the spectrum converge onto the same nonanalyticity in the thermodynamic limit, the effect of the λ_i nonanalyticity is lost as $L \to \infty$ and (20) and hence h_L remain analytic.

On the other hand a dynamical phase transition, as defined above, is only concerned with the eigenvalue λ_1. Therefore a dynamical phase transition does not necessarily coincide with a static phase transition. One very simple example would be if the two leading subdominant eigenvalues λ_1 and λ_2 crossed at some values of a control parameter. Then the gap would behave in a nonanalytic way but Z would be analytic.

Let us consider more explicitly the TASEP. From the exact solution of the TASEP [4, 15] the expression for Z_L, as defined by (19), is

$$Z_L = \frac{(\alpha\beta)^{L+1}}{\beta - \alpha} [\Phi_L(\alpha) - \Phi_L(\beta)] \tag{21}$$

where

$$\Phi_L(x) = \sum_{p=1}^{L} \frac{p(2L - p - 1)!}{L!(L - p)!} x^{-(p+1)} \tag{22}$$

and for L large

$$\Phi_L(x) \simeq \begin{cases} \dfrac{x(1-2x)}{[x(1-x)]^{L+1}} & x < \frac{1}{2} \\ \dfrac{4^L}{\sqrt{\pi L}} & x = \frac{1}{2} \\ \dfrac{x\, 4^L}{\sqrt{\pi}(2x-1)^2 L^{3/2}} & x > \frac{1}{2} \end{cases} . \tag{23}$$

Now consider, for example, the case $\alpha < 1/2$. As we increase β a first-order static phase transition occurs on the line $\beta = \alpha$ where the dominant contribution to (21) changes from $\Phi_L(\beta)$ to $\Phi_L(\alpha)$. Thus at the phase transition h_L defined in (20) is non-analytic. The subphase boundary is at $\beta = 1/2$ where the asymptotic behaviour of the subdominant contribution, $\Phi_L(\beta)$ changes. As this is a subdominant contribution to $\ln Z_L$, h_L remains analytic at the sub-phase boundary. At the dGE line there is no noticeable change in the asymptotic behaviour of Z_L and h_L is analytic.

5.2. Static vs dynamic transitions within various treatments of the TASEP

We illustrate further the distinctions between the static and dynamics phase diagrams by collecting exact results for the TASEP together with the predictions of various level of approximations such as mean field theory and domain wall theory.

Burgers Equation (Mean Field theory) We begin by considering a mean field description of the system that is given by the Burgers equation,

$$\partial_t \rho(x,t) = -(1-2\rho)\partial_x \rho + \frac{1}{2}\partial_x^2 \rho , \tag{24}$$

where $\rho(x,t)$ is a density field. Although the Burgers equation has been studied extensively in the literature, we are not aware of any treatment of the case with prescribed boundary reservoir densities. In the appendix we give the solution of (24) subject to the boundary conditions $\rho(0) = \alpha$ and $\rho(L) = 1 - \beta$, and arbitrary initial condition.

The results for the Burgers gap ε_B may be summarised as follows (restricting ourselves to the case $\alpha < 1/2$):

$$\text{For} \quad \beta < 1/2 \quad \varepsilon_B = -2|\alpha(1-\alpha) - \beta(1-\beta)| \tag{25}$$

$$\text{For} \quad \beta > 1/2 \quad \varepsilon_B = -\frac{(1-2\alpha)^2}{2} \tag{26}$$

The behaviour of the gap is plotted in Fig. 15. Note that a dynamical transition occurs at $\beta = 1/2$. Interestingly, it turns out that there is no change in the density profile at this value so, in fact, the mean field theory predicts a dynamical transition instead of a subphase boundary at $\beta = 1/2$. Thus even at the level of mean-field theory, the TASEP exhibits the phenomenon of a dynamic transition that is not accompanied by a static transition.
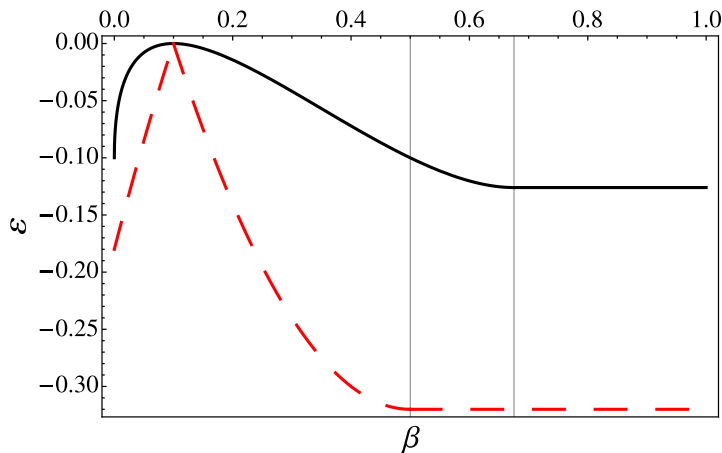
Figure 15. Comparison of the gap for $L \to \infty$ from the spectrum of the viscous Burgers equation (24) to the exact thermodynamic gap, for $\alpha = 0.1$ and $\beta_c \approx 0.675$.

Domain wall theory The predictions of domain wall theory were reviewed in Section 2.4. As we pointed out there, DWT gives a subphase boundary at $\beta = 1/2$ along with a dynamical transition: the distinction between the two phase diagrams is lost. However, in the subphases LDI and HDI, the DWT gives the correct dynamical gap to order $1/L^2$.

Exact results As was discussed in Section 2, the exact results for the stationary state [15,16] and the spectrum [20,21] reveal behaviour that is different from both mean-field and domain wall theory. In common with the latter, there is a static subphase boundary at $\beta = \frac{1}{2}$. Like the mean field theory, the location of the dynamic transition occurs at a distinct location to the static phase boundary. However, this location $\alpha_c(\beta)$ is nontrivial and is not predicted by either of the simpler theories. Moreover, the behaviour of the gap at the static transition point $\beta = \alpha$ differs between the mean-field and exact theories: in the former, the gap has a cusp, whereas in the latter it varies analytically.

6. Conclusion

In this work we have provided numerical evidence to confirm the existence of the dynamical transition line predicted by de Gier and Essler. Ultimately the evidence came from the approximate, but quantitatively reliable, DMRG technique.

To conclude, we now return to the main open question resulting from this work, namely that of the physical significance of the dynamical transition that takes place along the de Gier–Essler line. We remark again that, as was seen in Section 3, direct measurement of the gap in Monte Carlo simulations was very difficult. The nonanalyticity in the leading eigenvalue was barely detectable in the stochastic simulation data. We were therefore unable to identify, for example, whether the system relaxed to stationarity in a fundamentally different way either side of the transition line.

Given the success of the domain wall theory in predicting the gap in part of the phase diagram, it is tempting to believe that with some refinement it may be able to explain the dynamical transition and furthermore reveal the physics associated with it. For example, it has been noted in [21], that DWT may be modified to give the correct gap throughout the LD1′ region by simply imposing that the right domain density be $\rho^+ = 1 - \beta_c$ in this region. However DWT then no longer predicts a static subphase boundary at $\beta = 1/2$ and also the transition line $\alpha_c(\beta)$ is not predicted.

It may be that some knowledge of the form of the eigenvectors associated to the low lying states will allow an understanding of what occurs at the dynamical transition. It would be of interest to extend the DMRG studies to investigate the form of the eigenfunctions. Also recent analytic work by Simon [44], in which eigenvectors are constructed for the partially asymmetric exclusion process through the co-ordinate Bethe ansatz, may help to shed light on the matter.

Acknowledgments

Appendix A. DMRG algorithm for TASEP

In this appendix, we provide a step-by-step description of the DMRG algorithm used to obtain the results presented in Section 4.

In what follows we make use of three elementary transition matrices for the TASEP. With the ordering $(\_, \bullet)$ of single-site configurations we define

$$h_l = \begin{pmatrix} -\alpha & 0 \\ \alpha & 0 \end{pmatrix} \quad \text{and} \quad h_r = \begin{pmatrix} 0 & \beta \\ 0 & -\beta \end{pmatrix} \tag{A.1}$$

for the entry and exit of particles at the left and right boundary sites. In the bulk, and with the ordering $(\_\_, \_\bullet, \bullet\_, \bullet\bullet)$ of two-site configurations, we define

$$h_b = \begin{pmatrix} 0 & 0 & 0 & 0 \\ 0 & 0 & 1 & 0 \\ 0 & 0 & -1 & 0 \\ 0 & 0 & 0 & 0 \end{pmatrix} . \tag{A.2}$$

The DMRG algorithm now proceeds as follows.

0. *Initialise block transition matrices* We partition the system into two blocks, each of size ℓ. The transition matrix for the left block can be written as

$$M_L^{(\ell)} = h_l \otimes \mathcal{I}^{\otimes \ell - 1} + \sum_{k=1}^{\ell-1} \mathcal{I}^{\otimes k-1} \otimes h_b \otimes \mathcal{I}^{\otimes \ell - k - 1} , \tag{A.3}$$

where $\mathcal{I}$ is the 2×2 identity matrix. Likewise, for the right block one has

$$M_R^{(\ell)} = \sum_{k=1}^{\ell-1} \mathcal{I}^{\otimes k-1} \otimes h_b \otimes \mathcal{I}^{\otimes l-k-1} + \mathcal{I}^{\otimes \ell-1} \otimes h_r \ . \tag{A.4}$$

1. *Diagonalise the transition matrix for the entire system* The transition matrix for the entire system of size 2ℓ, $M^{(2\ell)}$, is given by

$$M^{(2\ell)} = M_L^{(\ell)} \otimes \mathcal{I}^{\otimes \ell} + \mathcal{I}^{\otimes \ell-1} \otimes h_b \otimes \mathcal{I}^{\ell-1} + \mathcal{I}^{\ell} \otimes M_R^{(\ell)} \ . \tag{A.5}$$

Now we diagonalise $M^{(2\ell)}$, first using the Arnoldi algorithm [45] (as implemented in the ARPACK package [46] and accessed using Mathematica) to find the left and right ground state eigenvectors $\langle \phi_0 |, |\psi_0 \rangle$. We also want to compute the gap and associated eigenvectors $|\psi_1\rangle$ and $\langle \phi_1 |$. Following [26], we find this can be done more accurately by 'shifting' the transition matrix through $M' = M^{(2\ell)} + \Delta |\psi_0\rangle \langle \phi_0 |$ sufficiently far that the gap is now the largest eigenvector of M'.

2. *Form reduced density matrices* The reduced density matrices are defined as

$$\rho_L = \frac{1}{4} \mathrm{Tr}_R (|\psi_0\rangle\langle\psi_0| + |\phi_0\rangle\langle\phi_0| + |\psi_1\rangle\langle\psi_1| + |\phi_1\rangle\langle\phi_1|) \tag{A.6}$$

$$\rho_R = \frac{1}{4} \mathrm{Tr}_L (|\psi_0\rangle\langle\psi_0| + |\phi_0\rangle\langle\phi_0| + |\psi_1\rangle\langle\psi_1| + |\phi_1\rangle\langle\phi_1|) \ . \tag{A.7}$$

Here Tr_L and Tr_R indicate a trace over the degrees of freedom in the left and right blocks respectively.

To be clear, let $\{|i\rangle_L\}$ and $\{|j\rangle_R\}$ be basis sets for the left and right blocks respectively. A state vector $|\psi\rangle$ across both blocks can then be expanded as

$$|\psi\rangle = \sum_{ij} c_{ij} |i\rangle_L |j\rangle_R \ . \tag{A.8}$$

The trace operation $\mathrm{Tr}_L(|\psi\rangle\langle\psi|)$ is then defined as

$$\mathrm{Tr}_L(|\psi\rangle\langle\psi|) = \sum_{jj'} \left(\sum_i c_{ij} c_{ij'} \right) |j\rangle_R \langle j'|_R \ . \tag{A.9}$$

Note that this is an operator acting only on the right block. The corresponding operation Tr_R is defined analogously.

3. *Diagonalise the density matrices and form a truncated basis set* We first find all eigenvalues and eigenvectors of the symmetric matrices ρ_L and ρ_R using a dense matrix diagonalisation routine from the LAPACK package [47], again accessed using Mathematica. We then form the matrices O_L and O_R that have as their columns the m eigenvectors with largest eigenvalues of ρ_L and ρ_R respectively. Then we construct projectors

$$P_L = O_L \otimes \mathcal{I} \quad \text{and} \quad P_R = \mathcal{I} \otimes O_R \tag{A.10}$$

that will be used in the renormalisation step below.

4. *Enlarge system* The left block is enlarged by adding a site at its right end. The transition matrix for this enlarged block is

$$\widetilde{M}_L^{(\ell+1)} = M_L^{(\ell)} \otimes \mathcal{I}^{\otimes 2} + \mathcal{I}^{\otimes \ell-1} \otimes h_b \ . \tag{A.11}$$

Likewise, the right block is enlarged by adding a site at its left:

$$\widetilde{M}_R^{(\ell+1)} = h_b \otimes \mathcal{I}^{\ell-1} + \mathcal{I}^{\otimes 2} \otimes M_R^{(\ell)}. \tag{A.12}$$

5. *Renormalise the transition matrices for the enlarged system* The renormalisation is performed by projection the enlarged transition matrices onto the subset of density matrix eigenstates that was retained in step 3. Formally, this is achieved by computing

$$M_L^{(\ell+1)} = P_L^T \widetilde{M}_L^{(\ell+1)} P_L \quad \text{and} \quad H_R^{(\ell+1)} = P_R^T \widetilde{M}_R^{(\ell+1)} P_R \ . \tag{A.13}$$

Note that after this transformation, the first ℓ sites of the system are no longer represented in the 'physical' basis (i.e., particle-hole configurations). However, the form of the projectors (A.10) ensures that the last site of the block *is* represented in the physical basis, which is essential for the expression (A.5) to be valid at each stage of the renormalisation.

6. *Return to step 1*, putting $\ell \to \ell + 1$.

Appendix B. Solution of the Burgers equation with fixed boundary densities

Here we solve the Burgers equation (i.e., the continuum limit of the TASEP within a mean-field theory)

$$\partial_t \rho(x, t) = -(1 - 2\rho)\partial_x \rho + \frac{1}{2}\partial_x^2 \rho \ . \tag{B.1}$$

subject to the boundary conditions $\rho(0) = \alpha$ and $\rho(L) = 1 - \beta$. We use the Cole-Hopf transformation [48], which involves the change of variable

$$\rho(x, t) = \frac{1}{2}\left[1 + \frac{\partial}{\partial x}\ln u(x, t)\right] \ . \tag{B.2}$$

Substituting into (B.1), and integrating with respect to x eventually yields

$$\frac{\partial}{\partial t}u(x, t) = \frac{1}{2}\frac{\partial^2}{\partial x^2}u(x, t) \ . \tag{B.3}$$

The boundary conditions on $\rho(x, t)$ transform to the conditions

$$u'(0, t) = (2\alpha - 1)u(0, t) \tag{B.4}$$
$$u'(L, t) = (1 - 2\beta)u(L, t) \ . \tag{B.5}$$

We proceed by finding the eigenfunctions $\phi_n(x)$ that satisfy

$$\frac{1}{2}\frac{\mathrm{d}^2}{\mathrm{d}x^2}\phi_n(x) = \lambda_n\phi_n(x) \tag{B.6}$$

along with the above boundary conditions at $x = 0$ and $x = L$. Thus given an initial condition $\rho(x, 0)$ the function $u(x, t)$ will be given by

$$u(x, t) = \sum_{n \geq 0} c_n e^{\lambda_n t}\phi_n(x) \tag{B.7}$$

where the coefficients c_n will depend on the initial condition. Inverting the Cole-Hopf transformation gives

$$\rho(x,t) = \frac{1}{2}\left[1 + \frac{\phi_0'(x)}{\phi_0(x)} + \frac{\sum_{n>0} c_n e^{(\lambda_n - \lambda_0)t}\phi_0(x)\left(\frac{\phi_n(x)}{\phi_0(x)}\right)'}{\sum_{n\geq 0} c_n e^{(\lambda_n - \lambda_0)t}\phi_n(x)}\right]. \tag{B.8}$$

The final term, involving the ratio of sums, vanishes as $t \to \infty$, as all λ_n with $n > 0$ exceed λ_0. Thus the stationary profile is

$$\rho(x) = \frac{1}{2}\left[1 + \frac{\phi_0'(x)}{\phi_0(x)}\right]. \tag{B.9}$$

We can define the Burgers gap, ε_B via the asymptotic rate of the exponential decay of the density profile to its stationary form, viz,

$$\varepsilon_B = \lim_{t\to\infty}\frac{\mathrm{d}}{\mathrm{d}t}\ln[\rho(x,t) - \rho(x)] = \lambda_1 - \lambda_0 . \tag{B.10}$$

The eigenfunctions given by (B.6) themselves take the form

$$\phi(x) = Ae^{\gamma x} + Be^{-\gamma x} \tag{B.11}$$

whence $\lambda = \frac{1}{2}\gamma^2$. The allowed values of γ are quantised due to the boundary conditions (B.4) and (B.5). We first look for solutions with $\lambda > 0$, i.e., real γ. Imposing the boundary conditions leads to the pair of equations

$$\gamma(A - B) = (2\alpha - 1)(A + B) \tag{B.12}$$

$$\gamma(Ae^{\gamma L} - Be^{-\gamma L}) = (1 - 2\beta)(Ae^{\gamma x} + Be^{-\gamma x}) . \tag{B.13}$$

These equations are consistent only if

$$\tanh(\gamma L) = \frac{2(1 - \alpha - \beta)\gamma}{(1 - 2\alpha)(1 - 2\beta) + \gamma^2} . \tag{B.14}$$

In the limit $L \to \infty$, the left-hand side approaches ± 1. The resulting equation has a solution $\gamma = 1 - 2\alpha$ if $\alpha < \frac{1}{2}$ and a solution $\gamma = 1 - 2\beta$ if $\beta < \frac{1}{2}$.

Solutions with a negative λ have purely imaginary $\gamma = ik$ (k real), and by following through the same procedure, one finds that the allowed values of k are the roots of

$$\tan(kL) = \frac{2(\alpha + \beta - 1)k}{k^2 - (2\alpha - 1)(2\beta - 1)} . \tag{B.15}$$

In the large-L limit, we find that $k \sim 1/L$, and hence the associated eigenvalues vanish as $1/L^2$ in the thermodynamic limit.

We can now state the $L \to \infty$ behaviour of the Burgers gap ε as α and β are varied. When both α and β are smaller than $\frac{1}{2}$, there are two isolated positive eigenvalues $\lambda = \frac{(2\alpha-1)^2}{2}, \frac{(2\beta-1)^2}{2}$. In this region, then, the gap behaves as

$$\varepsilon_B = -\frac{|(2\alpha - 1)^2 - (2\beta - 1)^2|}{2} = -2|\alpha(1 - \alpha) - \beta(1 - \beta)| . \tag{B.16}$$

Like the exact gap (4), this vanishes along the HD-LD coexistence line $\alpha = \beta < \frac{1}{2}$. However, unlike the exact gap, the mean-field gap has a nonanalyticity along this line.

If α or β is increased above $\frac{1}{2}$, one of the two solutions with positive λ ceases to exist, and the second-largest eigenvalue $\lambda_1 = 0$ in the thermodynamic limit. Hence then, the size of the gap is simply equal to the value of the largest eigenvalue. That is, within the low-density phase $\alpha < \frac{1}{2}, \beta > \frac{1}{2}$,

$$\varepsilon_B = -\frac{(1-2\alpha)^2}{2} \tag{B.17}$$

and within the high-density phase $\alpha > \frac{1}{2}, \beta < \frac{1}{2}$

$$\varepsilon_B = -\frac{(1-2\beta)^2}{2} \ . \tag{B.18}$$

The Burgers gap thus exhibits nonanalyticities along the coexistence line $\alpha = \beta < \frac{1}{2}$, and along the lines $\alpha < \frac{1}{2}, \beta = \frac{1}{2}$ and $\alpha = \frac{1}{2}, \beta < \frac{1}{2}$. Thus the dynamic phase diagram for the Burgers equation appears the same as the static phase diagram, Fig. 1(a), except that the subphase boundaries have become dynamical transition lines.

References

[1] T. M. Liggett. *Stochastic interacting systems: contact, voter, and exclusion processes.* Springer Verlag, Berlin, 1999.

[2] B. Derrida. An exactly soluble non-equilibrium system: the asymmetric simple exclusion process. *Phys. Rep.*, 301:65, 1998.

[3] O. Golinelli and K. Mallick. The asymmetric simple exclusion process: an integrable model for non-equilibrium statistical mechanics. *J. Phys. A: Math. Gen.*, 39:12679, 2006.

[4] R. A. Blythe and M. R. Evans. Nonequilibrium steady states of matrix-product form: a solver's guide. *J. Phys. A: Math. Theor.*, 40:R333, 2007.

[5] V. Popkov, L. Santen, A. Schadschneider, and G. M. Schütz. Empirical evidence for a boundary-induced nonequilibrium phase transition. *J. Phys. A: Math. Gen.*, 34:L45, 2001.

[6] C. T. MacDonald, J. H. Gibbs, and A. C. Pipkin. Kinetics of biopolymerization on nucleic acid templates. *Biopolymers*, 6:1, 1968.

[7] Y. Aghababaie, G. I. Menon, and M. Plischke. Universal properties of interacting Brownian motors. *Phys. Rev. E*, 59:2578, 1999.

[8] S. Klumpp and R. Lipowsky. Traffic of molecular motors through tube-like compartments. *J. Stat. Phys.*, 113:233, 2003.

[9] S. Chatterjee. Diffusion of a hydrocarbon mixture in a one-dimensional zeolite channel: An exclusion model approach. *Micropor. Mesopor. Mat.*, 125:143, 2009.

[10] K. Sugden, M. R. Evans, W. C. K. Poon, and N. D. Read. Model of hyphal tip growth involving microtubule-based transport. *Phys. Rev. E*, 75:031909, 2007.

[11] J. B. Martin and P. A. Ferrari. Stationary distributions of multi-type totally asymmetric exclusion processes. *Ann. Probab.*, 35:807, 2007.

[12] M. Evans, P. Ferrari, and K. Mallick. Matrix representation of the stationary measure for the multispecies TASEP. *J. Stat. Phys.*, 135:217, 2009.

[13] J. Krug. Boundary-induced phase transitions in driven diffusive systems. *Phys. Rev. Lett.*, 67:1882, 1991.

[14] B. Derrida, E. Domany, and D. Mukamel. An exact solution of a one-dimensional asymmetric exclusion model with open boundaries. *J. Stat. Phys.*, 69:667, 1992.

[15] B. Derrida, M. R. Evans, V. Hakim, and V. Pasquier. Exact solution of a 1D asymmetric exclusion model using a matrix formulation. *J. Phys. A: Math. Gen.*, 26:1493, 1993.

[16] G. Schütz and E. Domany. Phase transitions in an exactly soluble one-dimensional exclusion process. *J. Stat. Phys.*, 72:277, 1993.

[17] V. Popkov and G. M. Schütz. Steady-state selection in driven diffusive systems with open boundaries. *Europhys. Lett.*, 48:257, 1999.

[18] J. S. Hager, J. Krug, V. Popkov, and G. M. Schütz. Minimal current phase and universal boundary layers in driven diffusive systems. *Phys. Rev. E*, 63:056110, 2001.

[19] S. Mukherji and S. M. Bhattacharjee. Nonequilibrium criticality at shock formation in steady states. *J. Phys. A: Math. Gen.*, 38:L285, 2005.

[20] J. de Gier and F. H. L. Essler. Bethe ansatz solution of the asymmetric exclusion process with open boundaries. *Phys. Rev. Lett.*, 95:240601, 2005.

[21] J. de Gier and F. H. L. Essler. Exact spectral gaps of the asymmetric exclusion process with open boundaries. *J. Stat. Mech.: Theor. Exp.*, P12011, 2006.

[22] J. de Gier and F. H. L. Essler. Slowest relaxation mode in the partially asymmetric exclusion process. *J. Phys. A: Math. Theor.*, 41:485002, 2008.

[23] R. I. Nepomechie and F. Ravanini. Completeness of the Bethe ansatz solution of the open XXZ chain with nondiagonal boundary terms. *J. Phys. A: Math. Gen.*, 36:11391, 2003.

[24] R. I. Nepomechie. Functional relations and Bethe ansatz for the XXZ chain. *J. Stat. Phys.*, 111:1363, 2003.

[25] M. Dudzinski and G. M. Schutz. Relaxation spectrum of the asymmetric exclusion process with open boundaries. *J. Phys. A: Math. Gen.*, 33:8351, 2000.

[26] Z Nagy, C Appert, and L Santen. Relaxation times in the ASEP model using a DMRG method. *J. Stat. Phys.*, 109:623, 2002.

[27] R. M. Noack and S. R. White. *Density-Matrix Renormalization: A New Numerical Method in Physics*, chapter 2. Lecture Notes in Physics. Springer, 1999.

[28] S. R. White. Density matrix formulation for quantum renormalization groups. *Phys. Rev. Lett.*, 69:2863, 1992.

[29] U. Schollwöck. The density-matrix renormalization group. *Rev. Mod. Phys.*, 77:259, 2005.

[30] E. Carlon, H. Henkel, and U. Schollwöck. Density matrix renormalization group and reaction-diffusion processes. *Euro. Phys. J. B*, 12:99, 1999.

[31] R. A. Blythe and M. R. Evans. Lee-Yang zeros and phase transitions in nonequilibrium steady states. *Phys. Rev. Lett.*, 89:080601, 2002.

[32] M. R. Evans and R. A. Blythe. Nonequilibrium dynamics in low-dimensional systems. *Physica A*, 313:110, 2002.

[33] A. B. Kolomeisky, G. M. Schütz, E. B. Kolomeisky, and J. P. Straley. Phase diagram of one-dimensional driven lattice gases with open boundaries. *J. Phys. A: Math Gen.*, 31:6911, 1998.

[34] B. Derrida, M. R. Evans, and K. Mallick. Exact diffusion constant of a one-dimensional asymmetric exclusion model with open boundaries. *J. Stat. Phys.*, 79:833, 1995.

[35] D. T. Gillespie. Exact stochastic simulation of coupled chemical reactions. *J. Phys. Chem.*, 81:2340, 1977.

[36] T. P. Ryan. *Modern Regression Methods*. Wiley, Hoboken, NJ, 1997.

[37] C. Boldrighini, G. Cosimi, S. Frigio, and M. Grasso Nunes. Computer simulation of shock waves in the completely asymmetric simple exclusion process. *J. Stat. Phys.*, 55:611, 1989.

[38] P. A. Ferrari. Shock fluctuations in asymmetric simple exclusion. *Probab. Theory Rel.*, 91:81, 1992.

[39] B. Derrida, S. A. Janowsky, J. L. Lebowitz, and E. R. Speer. Exact solution of the totally asymmetric simple exclusion process: Shock profiles. *J. Stat. Phys.*, 73:813, 1993.

[40] S. R. White. Strongly correlated electron systems and the density matrix renormalization group. *Phys. Rep.*, 301:187, 1998.

[41] R. M. Noack and S. R. Manmana. Diagonalization- and numerical renormalization-group-based methods for interacting quantum systems. *arXiv:cond-mat/0510321v1*, 2005.

[42] R. A. Blythe. *Nonequilibrium phase transitions and dynamical scaling regimes*. PhD thesis, University of Edinburgh, 2001.

[43] E. Senata. *Non-negative matrices and Markov Chains*. Springer Series in Statistics. Springer,

New York, 1981.

[44] D. Simon. Construction of a coordinate bethe ansatz for the asymmetric exclusion process with open boundaries. *J. Stat. Mech.: Theor. Exp.*, P07017, 2009.

[45] G. H. Golub and C. F. van Loan. *Matrix Computations*. Johns Hopkins University Press, Baltimore, MD, third edition, 1996.

[46] R. Lehoucq, K. Maschhoff, D. Sorensen, and C. Yang. The ARPACK library. http://www.caam.rice.edu/software/ARPACK.

[47] The LAPACK library. http://www.netlib.org/lapack.

[48] W.A. Woyczyński. *Burgers-KPZ Turbulence*, chapter 3. Lecture Notes in Mathematics. Springer, 1998.